

## EIC 197 MHz CRAB CAVITY RF OPTIMIZATION\*

Zenghai Li<sup>†</sup>, SLAC, Menlo Park, CA, USA

Binping Xiao, Qiong Wu, Wencan Xu, BNL, Upton, NY, USA

J. R. Delayen, S. U. De Silva, Old Dominion University, Norfolk, VA, USA

R. Rimmer, JLab, Newport News, VA, USA.

### Abstract

Crab cavities, operating at 197 MHz and 394 MHz respectively, will be used to compensate the loss of luminosity due to a 25 mrad crossing angle at the interaction point in the Electron Ion Collider (EIC). Both crab cavities are of the RF Dipole (RFD) shape. To meet the machine design requirements, there are a few important cavity design considerations that need to be addressed. First, to achieve stable cavity operation at the design voltages, cavity geometry details must be optimized to suppress potential multipacting. Incorporating strong HOM damping in the cavity design is required for the beam stability and quality. Furthermore, due to the finite pole width, the multipole fields, especially the sextupole and the decapole terms, need to be minimized to maintain an acceptable beam dynamic aperture. This paper will present the RF optimization details of the 197 MHz cavity.

### INTRODUCTION

In the current EIC design, a large crossing angle of 25 mrad at the interaction region (IR) is required for fast separation of two colliding beams to minimize IR background and to ease the arrangements of IR beamline and detector components [1, 2]. Local crabbing scheme is adopted to recover the luminosity loss due to the crossing angle. A set of crab cavities with frequencies of 197 MHz and 394 MHz will be installed on each side of the detector. The RF dipole (RFD) [3], as shown in Fig. 1, is adopted for both the 197 MHz and 394 MHz crab cavities. The optimization of the 197 MHz cavity is required to meet the following design considerations. The beampipe aperture is 100 mm to accommodate the large beta function (1300 m) at the crab cavity region. The max peak surface fields are set to be 45 MV/m ( $E_{pk}$ ) and 80 mT ( $B_{pk}$ ) at the deflecting voltage of 11.5 MV. Strong HOM damping is essential to minimize the impedance contribution of the crab cavities. The deflecting field within the beam pipe aperture need to be highly uniform to maintain an acceptable beam dynamic aperture. Specifically, the field non-uniformity is dominated by the sextupole (b3) and decapole (b5) terms that need to be minimized. Further, the cavity geometry should be optimized to eliminate conditions of multipacting, especially around the operating voltage. In this paper, we present the results of the 197 MHz cavity optimization, focusing mostly on the multipacting and multipole field analysis and mitigations.

\* Work supported by Brookhaven Science Associates, LLC under Contract No. DE-SC0012704 with the U.S. Department of Energy, and by DOE Contract No. DE-AC02-76SF00515. This work used computer resources at the National Energy Research Scientific Computing Center.

<sup>†</sup>lizh@slac.stanford.edu

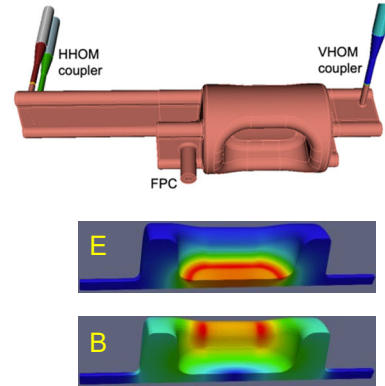


Figure 1: 197 MHz RFD cavity and field contour plots.

Table 1: 197 MHz RFD Cavity Parameters

Parameter	Value
Operating frequency [MHz]	197
1 <sup>st</sup> longitudinal HOM [MHz]	392
1 <sup>st</sup> transverse HOM [MHz]	342
R/Q [ $\Omega$ ] (with curved pole)	966
$V_T$ (MV/cavity)	11.5
$E_p$ (at $V_T=11.5$ MV) [MV]	45
$B_p$ (at $V_T=11.5$ MV) [mT]	81
Beam pipe aperture [mm]	100
Transverse dimension [mm]	587
Longitudinal dimension [mm]	922

### HOM DAMPING

The major RF parameters of the 197 MHz cavity is shown in Table 1. The operating mode in the RFD cavity is the fundamental mode. The lowest HOM mode is about 150 MHz higher in frequency which is advantageous for implementing the HOM damping. For impedance budget considerations [4], 2 IP are assumed in the hadron storage ring (HSR). Four 197 MHz crab cavities per side for IP-1 and five cavities per side for IP-2 (due to a larger crossing angle). That totals the number of 197 MHz cavities to twenty. The longitudinal impedance budget is 10.0 k $\Omega$  (circuit definition) per cavity. The transverse impedance budget per cavity are 0.132 M $\Omega$ /m and 0.66 M $\Omega$ /m respectively for the horizontal and vertical planes due to differences in beta functions. These impedance budget numbers were obtained by dividing the total impedance budgeted for the crab cavities by the number of cavities, which is a conservative assumption that all cavities are being identical. In reality, the HOM frequencies will deviate from cavity to cavity due to fabrication tolerances, which could loosen the impedance limit per cavity. Nevertheless, HOMs up to 2 GHz need to be adequately damped.

The HOM damping in the 197 MHz cavity is realized via two dogbone shaped waveguides that extract the HOM

power from the cavity. One of which is in the horizontal plane and one is in the vertical plane. The waveguides are matched to coaxial lines, 2 in horizontal and 1 in vertical, that are connected to the external coaxial loads. Two symmetrizing dogbone waveguide stubs are added to keep the field symmetry. They are also used as the coupling ports for the FPC (horizontal stub) and the field pickup (vertical stub). The dogbone waveguide has a cutoff of 335 MHz and is actively a high-pass filter for the horizontal HOMs. Certain length is needed before the waveguide is converted to coax to minimize fundamental power leakage. The dogbone waveguide on the vertical plane selectively rejects the operating mode. Thus only a short waveguide stub is needed before it is converted to a coax. The HOMs damping using these dampers are shown to be effective. The resulting HOM impedance is shown in Fig. 2. The total HOM power is estimated to be about 4.6 kW. Absorbing this level of HOM power by the three coaxial loads is feasible.

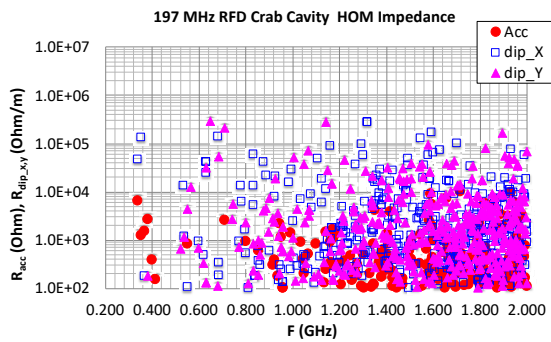


Figure 2: HOM impedances.

### MULTIPACTING ANALYSIS

Multipacting (MP) in superconducting cavity could strongly affect the RF processing and performance. Comprehensive MP analysis and design mitigation were carried out using Track3P [5]. Potential MP are identified by resonant trajectories at given deflecting voltages. The secondary yield (SEY) and the enhancement counter are both used to evaluate the strength of the MP. Trajectories with impact energies of high SEY indicates likely multipacting. Likewise, trajectories of high enhancement counter indicate strength of MP. The SEY curves in Fig. 3 were used for the MP analysis. The antenna of the FPC is of copper and the rest of the surfaces are of Nb.

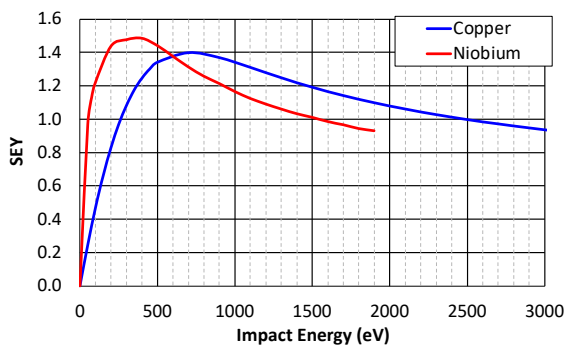


Figure 3: FEY curves for copper and Nb.

### Multipacting on Cavity

MP resonant trajectories were found in two areas in the cavity body. One is around the rounding edge of the end plate as shown in Fig. 4. The other is on the top surface of the cavity body as shown in Fig. 5.

The MP band in the rounding edge appeared to be sensitive to the end-plate tilt angle. A smaller tilt angle reduced both the MP bandwidth as well as the enhancement counter. The smaller angle (shown in green) was adopted for the current design. While the MP band was not totally eliminated with this tilt angle, the narrow band and lower strength will help improving the process time.

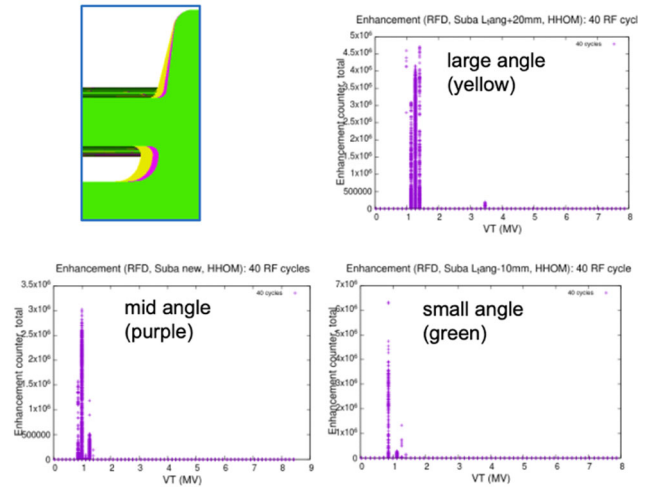


Figure 4: MP comparison at the end-plate corner.

The MP on the top surface was identified as of un-stable resonance MP. The resonant trajectories started at the center plane of the cavity and then drift to the side and disappear after about 40 RF cycles. The enhancement is low as the result of changing in impact energies of consecutive impacts toward the low SEY region. These un-stable resonances do not cause significant MP buildup.

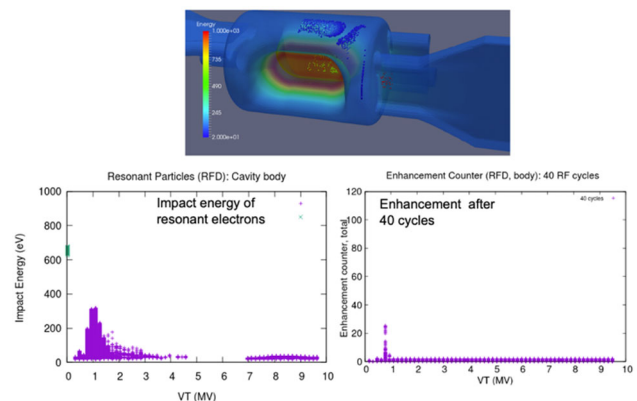


Figure 5: Non-stable resonant electrons in cavity that drift away after 40 cycles and is out of resonance, resulting in low MP enhancement.

### Multipacting in FPC Coupler Window

The coaxial window for the 197 MHz crab cavity FPC uses the same window design of the 591 MHz main cavity FPC [6, 7]. MP simulation has shown resonant trajectories existed in the choke region of the window box at power levels (traveling) above 750 kW (Fig. 6). To suppress the MP, Tin coating (good Tin with SEY <1.2) will be applied to the window assembly. It noteworthy to point out that the input power for the 197 MHz crab cavity is only up to 60 kW. There is no MP at power levels below 100 kW.

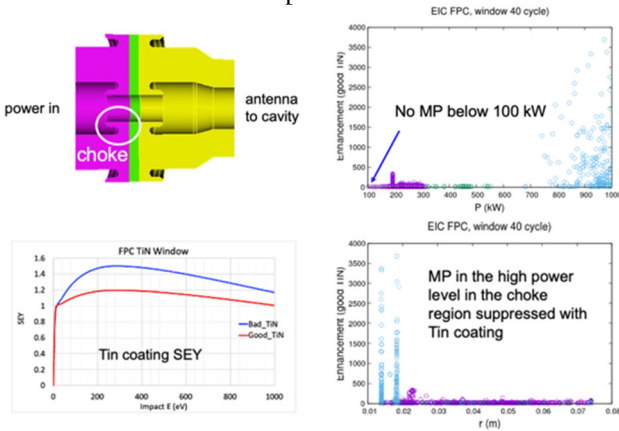


Figure 6: Multipacting in FPC window.

### Multipacting in FPC Coupler

The coaxial FPC coupler is positioned on the horizontal HOM coupler symmetrizing waveguide stub. The FPC couples to the cavity mode electrically via a e-probe. The FPC antenna is made of copper and is water cooled. The Qext of the FPC is 1.75e6. The nominal input power is about 10 kW. The maximum input power is 60 kW to have enough overhead for compensating potential microphonics and beam loading effects.

Both the 50 Ω FPC and 75 Ω FPC were analyzed for comparison. In the 50 Ω FPC, strong MP enhancement is found in a band from 7 MV to 9 MV as shown in Fig. 7. The resonances are located around the taper region between the coax and the window. This band is very close to the nominal operation voltage. A bias voltage of >1 kV is necessary to suppress this MP band.

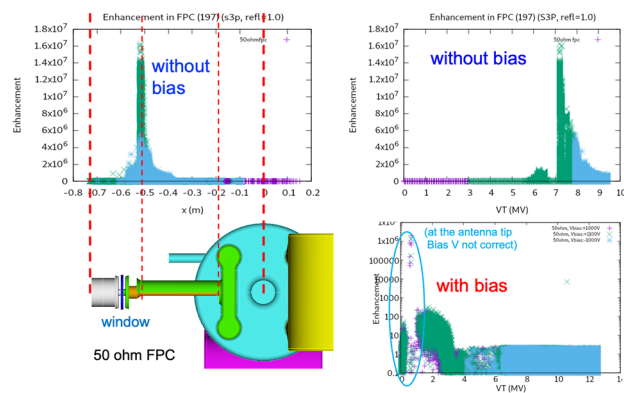


Figure 7: MP band in the 50 Ω FPC. Bias voltage > 1 kV is needed to suppress the MP.

In the 75 Ω FPC, resonant trajectories were found to exist in the similar location and similar deflecting voltages. However, the MP strength is much lower due to the low SEY of the corresponding impact energies, see Fig. 8. No bias voltage would be needed with the 75 Ω design. The inner conductor diameter of the 75 Ω design is about 0.66 time that of the 50 Ω design. Mechanical analysis has validated that both the strength and the implementation of water cooling with the reduced diameter antenna are feasible.

Both the 50 Ω and the 75 Ω FPCs would work abide bias voltage be applied in the 50 Ω design. The 75 Ω FPC is less susceptible to MP and no needing of bias, thus is chosen for the 197 MHz crab cavity. The mechanical implementation of the 75 Ω FPC will keep the bias option, but not expected to be utilized in operation.

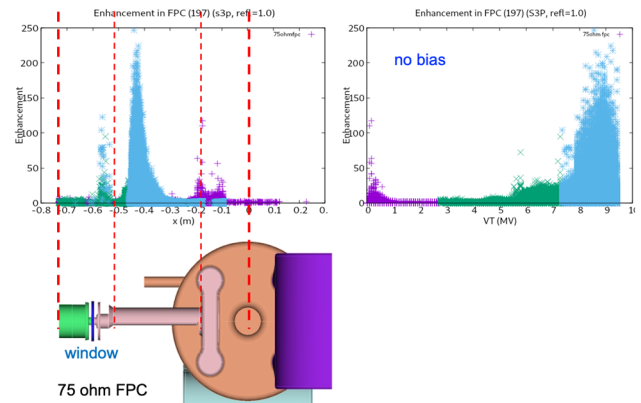


Figure 8: Low MP enhancement counter in the 75 Ω FPC.

### Multipacting in the HOM Couplers

The evanescent fields in the dogbone HOM waveguides that may create resonant trajectory conditions for MP. In the VHOM coupler, the evanescent field only extends to a very short distance into the coupler as the coupler naturally rejects coupling to the cavity mode. There is no MP in the VHOM coupler waveguide. The high enhancement MP shown in the top two plots in Fig. 9 are the MP in the end-plate rounding corner (similar to Fig. 4). In the HHOM coupler, the evanescent field extends exponentially to a longer distance in the waveguide. This field supports resonant trajectories at the waveguide regions that varies with the deflecting voltage. However the impact energies of the resonant trajectories do not fall in the high SEY range. As a result, they do not produce high enhancement (Fig. 9, bottom). The MP does not seem to be a concern in both the VHOM and HHOM couplers.

Content from this work may be used under the terms of the CC BY 4.0 licence (© 2023). Any distribution of this work must maintain attribution to the author(s), title of the work, publisher, and DOI

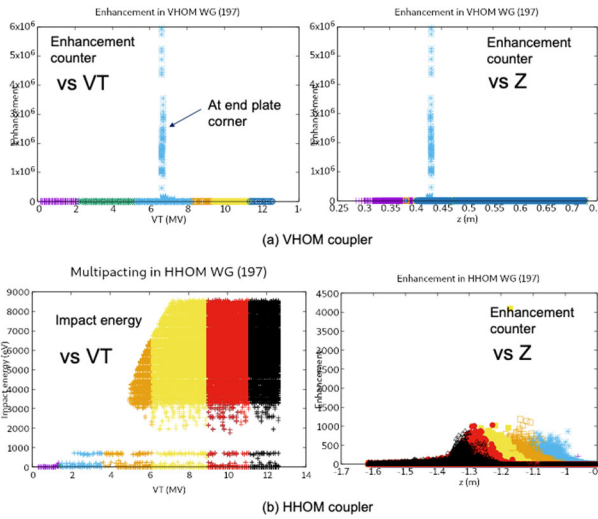


Figure 9: Impact energy and enhancement counters of resonant trajectories. Top: VHOM; bottom: HHOM.

## MULTIPOLE FIELDS

Finite pole width resulted in non-uniform deflecting fields in the deflecting gap. The sextupole (b3) and decapole (b5) terms defined in Eq. (1) need to be minimized to reduce their effects on the beam dynamic aperture [8].

$$V_{acc}(r, \phi) = \sum_n V_{acc}^n r^n \cos(n\phi)$$

$$V_{\perp}(r, \phi) = \sum_n \frac{nc}{\omega} V_{acc}^n r^{n-1} (\hat{u}_r \cos(n\phi) + \hat{u}_\theta \sin(n\phi)) \quad (1)$$

$$b_n = \frac{nc}{\omega} V_{acc}^n$$

The preliminary requirements of the b3 and b5 are listed in Table 2. With a simple flat pole surface, the b3 was found to be more than 7 times higher than the requirement while the b5 is well below the threshold. Incorporating curved surface in the pole profile is necessary to minimize the multipole fields. The first approach was to add a simple elliptical curvature to the pole surface. However, the b3 and b5 turned out to have opposite derivatives with respect to this simple curvature. Adding a flat section in the middle as shown in Fig. 10 helps to balance the sensitivities of b3 and b5, which allows both to be minimized. The optimized results of b3 and b5 are shown in Table 2.

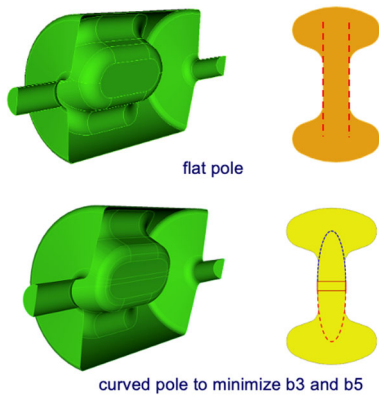


Figure 10: Minimizing the b3 and b5 multipole terms by introducing a curved pole profile.

Table 2: Comparison of b3 and b5 (for VT=25.8 MV) between flat and optimized curved pole profiles. The peak surface fields are calculated for VT=11.5 MV.

	B3 (T/m)	B5 (T/m <sup>3</sup> )	Es (MV/m)	Bs (mT)
Preliminary requirements	0.18	220		
Flat pole	1.362	70.7	44.5	79.1
curved pole	0.023	79.7	44.9	81.3

The pole shape need will be machined to achieve a high profile accuracy to keep b3 and b5 under control. The e-beam welding could result in misalignments of the poles in the level of sub-millimeters. These fabrication errors could potentially be detrimental to the field uniformity. We have analyzed the effects of typical misalignment errors of the poles on the b3 and b5 multipoles. The results are shown in Table 3. The tolerance of b3 and b5 to the pole misalignment appears to be quite insensitive. The approach to incorporate an accurate curved pole profile to minimize the b3 and b5 are shown to be achievable.

Table 3: Effects of pole misalignments on b3 and b5. Both b3 and b5 are calculated for VT=25.8 MV.

Misalign of one pole on +x side	b3 (T/m)	b5 (T/m <sup>3</sup> )	
rotate 0.2 deg about z: (dy at rcav ~ 1 mm)	0.0230	79.9	
rotate 0.2deg about y: (z ends of pole dx ~ ± 1 mm)	0.0257	80.0	
shift in y: dy=0.5 mm	0.0230	80.2	
shift in z: dz=0.5 mm	0.0231	79.8	

## SUMMARY

Comprehensive modeling of the HOM damping, multipacting and mitigation, and multipole fields compensation have been carried out. The results have shown that the 197 MHz cavity design would meet the design requirements for the EIC.

## REFERENCES

- [1] C. Montag *et al.*, “Design Status Update of the Electron-Ion Collider”, in *Proc. IPAC'21*, Campinas, Brazil, May 2021, pp. 2585-2588.  
doi:10.18429/JACoW-IPAC2021-WEPAB005
- [2] D. Xu, Y. Luo, and Y. Hao, “Combined effects of Crab Dispersion and Momentum Dispersion in Colliders with Local Crab Crossing Scheme”, *arXiv*, 2022.  
doi:10.48550/arXiv.2205.03462
- [3] Z. Li *et al.*, “FPC and Hi-Pass Filter HOM Coupler Design for the RF Dipole Crab Cavity for the LHC HiLumi Upgrade”, in *Proc. IPAC'15*, Richmond, VA, USA, May 2015,

pp. 3492-3495.

doi:10.18429/JACoW-IPAC2015-WEPWI004

[4] B. P. Xiao *et al.*, “HOM Damper Design for BNL EIC 197 MHz Crab Cavity”, in *Proc. SRF'21*, East Lansing, MI, USA, Jun.-Jul. 2021, pp. 624.

doi:10.18429/JACoW-SRF2021-WEPCAV014

[5] Z. Li, L. Ge, C.-K. Ng, and L. Xiao, “Recent Developments and Applications of Parallel Multi-Physics Accelerator Modeling Suite ACE3P”, in *Proc. NAPAC'19*, Lansing, MI, USA, Sep. 2019, pp. 888-891.

doi:10.18429/JACoW-NAPAC2019-WEPL04

[6] W. Xu *et al.*, “Broadband high power rf window design for the BNL Electron Ion Collider”, *Phys. Rev. Accel. Beams*, vol. 25, p. 061001, 2022.

doi:10.1103/PhysRevAccelBeams.25.061001

[7] W. Xu, “High power coupler development for EIC”, BNL, Upton, NY, USA, BNL-221833-2021-TECH, EIC-TSD-TN018, Jul. 2021.

[8] Q. Wu, S. U. De Silva, Z. Li, Y. Luo, and B. P. Xiao, “EIC Crab Cavity Multipole Analysis and Their Effects on Dynamic Aperture”, in *Proc. IPAC'22*, Bangkok, Thailand, Jun. 2022, pp. 66-69.

doi:10.18429/JACoW-IPAC2022-MOPOST009